Extending thermal stability of short-living soliton states in silicon nitride microring resonators

D. Grassani, H. El Dirani, F. Sabattoli, L. Youssef, C. Petit-Etienne, S. Kerdiles, Erwine Pargon, M. Liscidini, C. Sciancalepore, D. Bajoni, et al.

Extending thermal stability of short-living soliton states in Silicon Nitride microring resonators

D. Grassani[1,5,*], H. El Dirani[2,6], F. A. Sabattoli[1,7], L. Youssef[3,8], C. Petit-Etienne[3], S. Kerdiles[2], E. Pargon[3], M. Liscidini[1], C. Sciancalepore[2,9], D. Bajoni[4], and M. Galli[1]

[1]*Dipartimento di Fisica, Università di Pavia, Via Bassi 6, 27100 Pavia, Italy*
[2]*Univ. Grenoble Alpes, CEA-LETI, 38054 Grenoble cedex, France*
[3] *Université Grenoble Alpes, CNRS, CEA/LETI-Minatec, Grenoble INP, LTM, F-38054, Grenoble, France*[4]*Dipartimento di Ingegneria Industriale e Informazione, Università di Pavia, via Ferrata 1, 27100 Pavia, Italy*
[5]*Currently with the Centre Suisse d'Electronique et de Microtechnique (CSEM), 2000 Neuchâtel, Switzerland*
[6]*Currently with STMicroelectronics, 38926 Crolles Cedex, France*
[7]*Currently with Advanced Fiber Resources Milan, via Fellini 4, 20097 San Donato Milanese (MI), Italy*
[8]*Currently with ENSIL-ENSCI, Centre Européen de la Céramique, 12 rue Atlantis, 87068 Limoges, France*
[9]*Currently with SOITEC SA, Parc technologique des Fontaines, Chemin des Franques, 38190 Bernin, France*
**davide.grassani@csem.ch*

Abstract: Dissipative Kerr Solitons in microresonators enable chip integration of sources for low-noise optical pulse trains with high repetition rates, finding applications in optical communication, distance measurement, spectroscopy and radiofrequency generation. However, the most common silicon-Extending based platforms have a large thermo-optic coefficient which often results in very short living soliton states, difficult to access by simple laser tuning. Here we extend the soliton lifetime in SiN far beyond what is imposed by the thermal constant of the resonator by using an auxiliary resonance. We access thermally stable soliton states by slow wavelength or thermal tuning with no need of any pump modulation, feedback loop or additional lasers.

1. Introduction

An Optical Frequency Comb (OFC) can be generated in an optical microresonator (microcomb) exhibiting Kerr nonlinearity by cascaded four-wave mixing [1,2], after reaching the threshold of parametric oscillations [3]. The OFC can eventually turn into a Dissipative Kerr Soliton (DKS) state [4], when a double balance between dispersion with nonlinearity and losses with parametric gain is obtained under continuous wave (cw) pumping condition [5]. Similarly to a mode-locked laser, a DKS has a broadband spectrum of low noise and equidistant phase-locked frequency lines in the spectral domain [6] and short pulses in the time domain [7]. However, microresonator-based DKS shows high repetition rates (from tens of Gigahertz to Terahertz), and they have been employed in applications usually beyond the reach of mode-locked lasers, especially in the field of spectroscopy [8–11], metrology [12–15], optical communication [16,17], distance measurement [18], radiofrequency and microwave generation [19]. Over the past years, soliton microcombs have been investigated in different materials and geometries, notably magnesium fluoride (MgF_2) [6,20,21] and microtoroids in silica [22,23] , or microring resonators in hydex [24,25], silicon [9,26] and silicon nitride (SiN) [12,27–29]. Among all the different platforms, SiN microrings have been widely used thanks to their planar photonic integration with access waveguides, large optical nonlinearity, ease of dispersion engineering, and large transparency window: spanning from the visible to the mid-infrared range, with negligible absorption in the telecommunication band region.

When a DKS state forms, part of the laser power coupled to the resonator circulates in the cavity as one or more spatial and temporal localized pulses with high peak power, accompanied by a remaining cw background. Such pulses lead to a larger Kerr effect and therefore a larger detuning of the resonance of the microcavity compared to the detuning of the cavity resonance due to the cw background. This implies that two resonance frequencies coexist at the same time: the soliton resonance (*S*-resonance) and the cavity resonance (*C*-resonance), with the former exhibiting a larger red-shift with respect to the cold cavity frequency than the latter. Therefore, a DKS state can only be accessed by operating in the red-detuned condition with respect to the cavity resonance. In principle, such a condition can be accessed by sweeping the laser frequency across the cavity mode from the blue to the red, passing through the noisy modulation instability (MI) regime of the OFC [6]. However, SiN exhibits a large thermo-optic coefficient, which makes it extremely challenging to keep the cavity in thermal equilibrium in the red-detuned condition [30]. In fact, when the pump laser wavelengths is larger than the cavity wavelength, the power coupled to the cavity drops abruptly, causing the resonator to cool-down and its resonances to blue shift with a characteristic time, which is inversely proportional to the thermo-optic coefficient of the microresonator and the amount of pump power absorbed by different loss mechanisms, such as multiphoton absorption processes [31] and localized defect states [32]. The lifetime of a DKS state lies within

such characteristic time, and it might vary depending on the quality factor (Q) of the resonator and the specific deposition process of SiN. In practice, the soliton lifetime in high-Q SiN resonators is usually too short (< 500 ns) for the laser tuning system to follow the resonance, thus a simple laser tuning rarely results in stable soliton microcomb formation.

Several strategies have been investigated to stably accessing DKS in microresonators when a simple frequency sweep is not a solution. Fast pump modulation schemes, such as the power kicking method [33], consist in a fast increase of the pump intensity when it enters the red-detuned regime in order to keep the resonator at thermal equilibrium. This can be done by a combination of acousto and electro-optic modulators together with feedback loops. More recently, slow pump modulation has shown to be a viable method to access DKS in SiN by slow frequency tuning. In fact, when the spectrum of the pump laser consists of two frequency lines spaced few linewidths of the resonator, the cool-down of the system and the subsequent recoil of the resonance can be stopped by the second, blue-detuned, frequency line that couples to the same mode [34]. Analogously, the resonator can be stabilized by an auxiliary laser which is coupled to a different mode. This is usually obtained by a far detuned [22] or a counter propagating [24,27] additional laser, for easier filtering. In a similar way, it has been shown that a mode on the red-detuned side of the pump resonance can mitigate the thermal requirements for low-order soliton formation [35].

In this work we follow a different strategy and we use two adjacent orthogonal modes to extend the soliton lifetime of a SiN microresonator, allowing to reach the DKS state by slow (or manual) tuning of the pump laser. We show that the improved thermal stability allows for soliton mode-locking the microcomb by simple thermoelectric cooling of the entire chip, using a fixed frequency laser, greatly reducing the resource requirements with respect to common methods. We perform systematic measurements to understand the likelihood of single soliton generation and its dependence on the splitting of the modes and total coupled power. Then, we assess the possibility to access single DSK by backward tuning technique when the microcomb is generated on a high-order soliton state.

2. Working principle and experimental set-up

The working principle is sketched in Fig.1a. Let's consider that the DKS is generated on the TE mode and that the TE cavity resonance (*C*-resonance TE) is blue-shifted with respect to the nearest TM one (*C*-resonance TM). Also, let's consider the laser to be linearly polarized such that part of its power couples to the TM mode. By progressively red detuning the laser, the optical power is first coupled to the *C*-resonance TE, causing a red shift of all the resonances of the ring due to self and cross-phase modulation and the thermo-optic effect. Also, a noisy comb is generated by cascaded four-wave mixing. Once the laser is red detuned from the *C*-resonance TE, the intracavity power suddenly drops, and the resonances undergo a first instantaneous blue-shift due to a reduction of the nonlinear phase shift. At this point, providing the frequency difference between the *C*-resonances TE and TM is smaller than this blue-shift, the power coupled into the TM mode of the waveguide enters the *C*-resonance TM *before the cavity cools down*. Therefore, we use an auxiliary resonance (*C*-resonance TM) to keep the resonator in thermal equilibrium and access the soliton state in the TE mode.

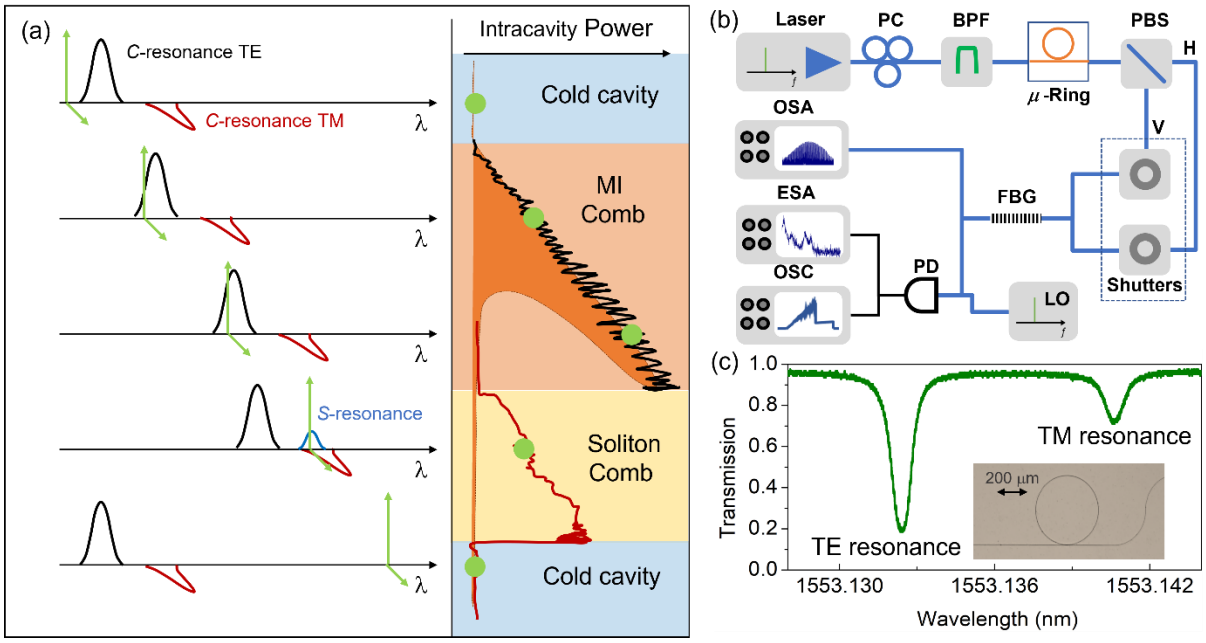

Figure 1 in a) on the left it is schematically shown the relative position of the pump laser with respect to the cavity TE (black) and TM (red) resonances for different position of the laser tuning. The TE S-resonance (blue) is shown for the system is in the red detuned regime. On the right, it is schematically shown the corresponding intracavity power of the resonators for the quasi-TE (black) and quasi-TM (red) modes. Green dots are placed in correspondence of the laser detuning conditions reported on the left. In b) it is detailed the experimental set-up where PC is polarization controller, BPF is Band-Pass-Filter, FBG is Fiber Bragg Grating, LO is local oscillator, PD is photodetector, OSA is Optical spectrum analyzer, ESA is Electrical spectrum analyzer and OSC stands for oscilloscope. H and V stand for horizontal and vertical polarization. Figure c) shows a transmission spectrum of the selected resonances taken with the pump laser polarized as in the experiment for soliton generation. The inset is an optical microscope image of the sample under test.

The experimental setup employed to access the DKS regime is reported in Figure 1b. A tunable, cw, external cavity laser (ECDL) (Santec TSL 710) passes through an Erbium Doped Fiber Amplifier (EDFA)(Keopsys CEFA-C-PB-HP) to reach the hundred-milliwatt level needed for DKS formation. Light is injected into the bus waveguide by means of a collimation/focusing lens pair. The same lens pair is used for collecting the light out of the chip. The laser polarization is selected via an in-fiber polarization controller. Before entering the sample, we filter out the amplified spontaneous emission of the laser with a bandpass filter. At the output of the chip a fiber-based polarizing beam splitter separates vertically polarized light (*V*), coming from light coupled and generated into the quasi-TM mode of the ring, from the horizontally polarized light (*H*), coming from the light coupled and generated into the quasi-TE mode. The *V* and *H* outputs are then sent to a first 50/50 fiber coupler. At one output of the coupler, the laser line is attenuated by a Fiber Bragg Grating (FBG). At the output of the FBG, a second 50/50 coupler routes the signals to an optical spectrometer and a fast InGaAs photodetector (Newport Model 818-BB-35F). The electrical signal from the photodetector is sent to a high bandwidth oscilloscope and an electrical spectrum analyzer (ESA). Also, a second CW ECDL is mixed via a 90/10 coupler to the light generated from the chip, acting as local oscillator (LO) for heterodyne measurements.

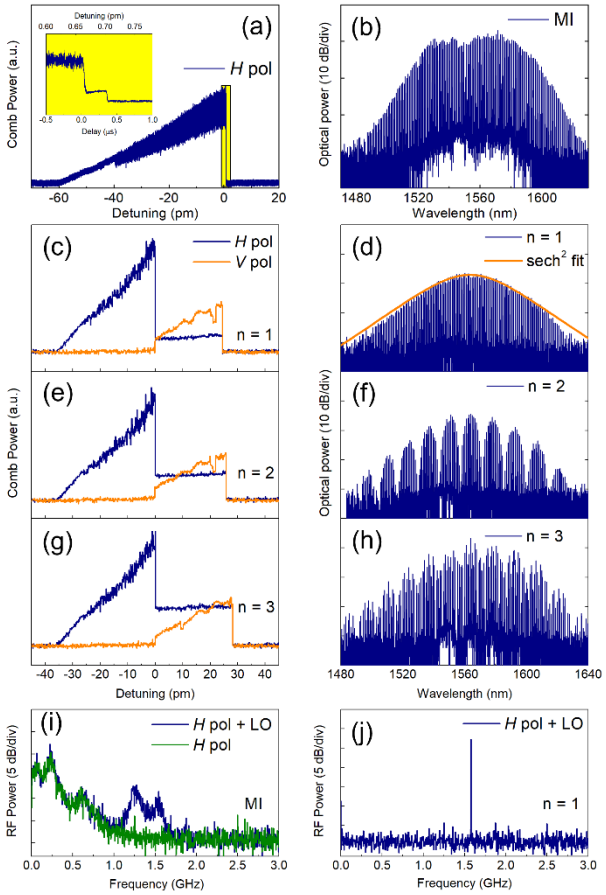

Figure 2 Panel a) shows the oscilloscope trace of the comb power as a function of the detuning between the laser and the C-resonance TE when the pump is entirely coupled on the quasi-TE mode. The inset is a zoomed view of the part of the trace highlighted in yellow, showing the duration of the soliton step. Panel b) shows the optical spectrum of the trace in panel a) just on the H polarization output. Panels c), e) and g) show the traces when about 20% of the pump power is coupled to the quasi-TM mode for n = 1,2 and 3 soliton states. Panels d), f) and h) show the optical spectrum just on the H polarization output for n = 1,2 and 3, correspondingly. Panels i) and j) show the beatnote in the RF spectrum, collected on the ESA, for the case of MI comb and n=1 DKS, respectively. To increase readability, we set detuning = 0 at the point where the system enters the red-detuned regime

The sample is fabricated by the twist and grow method from in the cleanroom facilities of CEA-Leti in Grenoble (…).
The fabrication starts with a 200mm silicon substrate, which is oxidized over 3µm. The deposition of the 800nm-thick, high-strain film of stoichiometric Si3N4 is done using Low Pressure Chemical Vapor Deposition (LPCVD) at 780°C. The process is performed following the twist-and-grow method [Ref1: H. El Dirani et al., « Crack-Free Silicon-Nitride-on-Insulator Nonlinear Circuits for Continuum Generation in the C-Band », IEEE Photonics Technol. Lett., vol. 30, no 4, p. 355 358, févr. 2018, doi: 10.1109/LPT.2018.2790045.], [Ref2: H. El Dirani et al., « Ultralow-loss tightly confining Si 3 N 4 waveguides and high-Q microresonators », Opt. Express, vol. 27, no 21, p. 30726, oct. 2019, doi: 10.1364/OE.27.030726.]: a two-steps deposition of 400nm Si3N4 with wafer rotation of 45° is apply to avoid possible cracks and film delamination due to the high tensile strain. The film is then patterned using 248nm Deep Ultra-Violet photolithography and dry etching. The Si3N4 film on the backside is removed to release the strain. After that, the SiN waveguide undergoes a series of thermal annealing in O2, H2 and N2 atmospheres (ref 2]). The waveguides are then encapsulated using High Density Plasma (HDP) oxide deposition. Finally, the dyes are separated by combining : a deep etching of large trenches through the oxide and the silicon substrate followed by saw dicing to complete the dye separation. This procedure enables an optical quality facet for edge fiber coupling.???

The ring has a radius of 200 micron and its waveguide has a width of 1.7 µm and height of 0.8 µm. The microring is critically coupled to the bus waveguide via a point coupler featuring a gap of 550 nm. The entire

ring is thermally stabilized by means of a thermoelectric cooler (TEC) placed under the whole chip and driven by a feedback control loop. Figure 1c shows the oscilloscope trace of a low-power transmission spectrum of the employed orthogonally polarized resonances. We coupled about 78% of the total input power on quasi-TE mode and about 20% on the quasi-TM mode. The resonances are about 8 pm far apart and feature loaded quality factors $Q_{TE} = 2 \cdot 10^6$ and $Q_{TM} = 1.5 \cdot 10^6$.

3. Results

3.1 Extending soliton lifetime

We investigated the soliton lifetime by recording the power exiting from *H* and *V* polarizations on the oscilloscope, after being filtered by the FBG, during a wavelength scan (from blue to red) of the pump laser. At first, to assess the soliton lifetime of the system operating in the usual single-pump polarization configuration, we coupled about 245 mW entirely on the quasi-TE mode of the access waveguide. Figure 2a reports the power generated in the comb as a function of the detuning of the pump laser with respect to the pump resonance. The trace reproduces the typical behavior of noisy OFC formation, where the triangled shape reflects the bistability of the resonator, as a consequence of the thermal and nonlinear phase shift [30]. In the inset of Figure 2a we show a zoom of the main plot, in which we can observe that the soliton lifetime is less than 500 ns. The speed of the laser scanning was 100 nm/s for this specific trace, but we obtained similar results with values from 1 to 100 nm/s. It is therefore nearly impossible to access the soliton state by manual tuning or sweeping the laser grating. Indeed, as a steady, stable state we can just access a noisy MI comb that features the spectrum shown in Figure 2b. When we couple about 20% of the pump power to the quasi-TM mode of the waveguide, as in Figure 1b, the traces show substantial differences with respect to Figure 2a. First, the bistability range of the TE *C*-resonance is reduced from 60 to 40 pm. This is due to the reduced power coupled into the quasi-TE mode. More importantly, the power detected on the *V* polarization is nonzero and starts to increase when the pump laser exits the TE *C*-resonance (red-detuned regime). Further red tuning of the pump laser results in an increase of the power coupled to the TM resonance, with subsequent nonlinear power transfer from the pump to the sidebands created by cascaded FWM. Crucially, at this stage the power detected from the *H* polarization does not go to zero, indicating the system has achieved the DKS state [6]. The value at which the power on the *H* polarization stabilizes depends on the number of solitons (n) circulating in the ring. This is clearly shown in Fig. 2c, e and g, where the steps observed in the *H* polarized outputs have different heights, and their optical spectra change accordingly, as shown in Figures 2d, f, and h. In particular, the envelop of the comb of Fig. 2d fits well a sech^2 curve, which is the expected result for a DKS state with only one soliton circulating in the resonator (n = 1). The TM resonance shows a bistability behavior too, and a further red shift of the pump results in an abrupt drop of the coupled power inside the resonator. Interestingly, the lifetime of the DKS state in the quasi-TE mode corresponds to the entire bistability range of the TM resonance, despite the change in the temperature of the resonator. This indicates that once formed, the DKS regime is robust against changes in the environmental conditions, allowing one to greatly extend the soliton lifetime. Considering that for the traces in Fig. 2 (c), (e), (g) the employed tuning speed is of 1 nm/s, the soliton lifetime now results to be about 20 ms, that is more than 40 times longer than in the case of Fig. 2(a). This time is sufficient to achieve the DKS regime by manual laser tuning. Also, we investigated the coherence of the generated comb by heterodyne detection using an additional CW laser, tuned near one of the comb lines, as a local oscillator. Figure 2i shows the RF spectrum of the system when it is in the MI state. The spectrum is characterized by a large low-frequency noise (< 1 GHz) and a broad beat note around 1.3 GHz. When looking at the RF spectrum operating the comb in the n = 1 soliton state (Figure 2 j)), the background noise greatly reduces [7] and a narrow beat note with improved SNR arises.

3.2 Likelihood of multi-soliton states

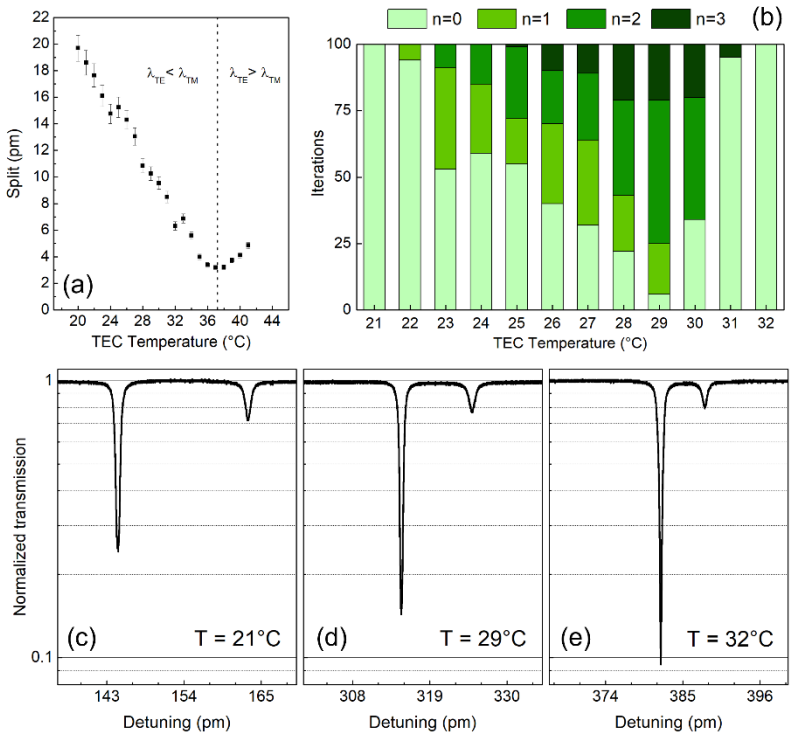

Figure 3 Panel a) shows the splitting between the C-resonance TE and TM as a function of the chip temperature. Panel b) shows the occurrence of soliton states with n = 1,2 and 3 and the failure of DKS state generation (n = 0) as a function of the chip temperature. Panels c), d) and e) shows the spectra of the pump and auxiliary resonances as a function of the laser detuning from the starting point of the wavelength scan (1552.985 nm).

The formation of DKS is a chaotic process starting from noisy MI state. It is thus very hard to predict how many solitons there will be in the final state. For instance, in our system, we can achieve DKS with n = 1,2,3. Nevertheless, there are few physical arguments that can help in understanding which soliton state is more likely to happen. In this section we investigate the dependency of the soliton number on the splitting of the TE and TM resonances and total power coupled to the resonator.

We control the splitting between the TE and TM *C*-resonances by changing the temperature of the thermoelectric cooler beneath the chip. In fact, the quasi-TE and quasi-TM modes have different overlap with the cladding. Then, considering that SiO_2 has a lower thermo-optic coefficient than SiN, this results in a different spectral shift of the TE and TM *C*-resonances for a given change in temperature. In Fig. 3a we report the resonance splitting as a function of the TEC temperature: at lower temperature, the splitting linearly reduces by increasing the temperature at a rate of about -1 pm/°C. This means that the quasi-TE mode has a higher thermo-optic coefficient with respect to the quasi-TM mode. This agrees with the fact that the quasi-TM mode has a larger field overlap with the silica cladding. We consider a temperature range from 20 °C to 37 °C, further increase in temperature above 42 °C results in swapping the resonances, with the TM *C*-resonance which is blue-shifted with respect to the TE one. In Figure 3 b) we show the statistics of DKS formation with n = 1,2 and 3 collected over 100 iterations for each temperature step of 1 °C between 21 °C and 32 °C. The results show that, for a too low temperature, the splitting is too large, and the TM resonance is too far to be excited when the cavity cools down. By reducing the splitting, the power coupled into the TM resonance increases, together with the probability of DKS generation and states with higher soliton number. It is interesting to notice that the minimum splitting at which the DSK start to happen is about 20 pm, which is roughly half the bistability range reported in Figure 2 c), e) and g) for the TE *C*-resonance. This value corresponds to the instantaneous recoil of the resonances, which solely depends on the reduction of the nonlinear phase shift, after the loss of power inside, the cavity but it does not include the thermo-optic contribution. Accordingly to the model presented in [35], the increased likelihood of higher soliton number generation when reducing the splitting can be qualitatively understood by the fact that, for a fixed thermo-optic coefficient, the smaller is the splitting, the lower is the recoil of the resonances before part of the light is coupled to the TM mode. For smaller detuning, the power level remaining in the TE resonance is higher, which can therefore sustain a higher soliton number.

Interestingly, the probability of soliton generation abruptly drops at 31 °C, when the splitting is around 6 pm. This can be explained by looking at the transmission spectra of the resonances reported in Figure 3 (c) and (e). In fact, by increasing the temperature we see as the TE and TM resonant modes start to couple. The coupling of

the modes can be due do waveguide imperfection, especially at the directional coupler point, and it is confirmed by the typical avoided mode crossing feature that the two modes exhibit in Fig. 3a at around 37°C. When coupled, the eigenmodes of the resonators are no more given by the quasi-TE (H) and quasi-TM (V) polarizations, but by their linear superposition: the Diagonal ($D = 1/\sqrt{2}(H + V)$) and Anti-diagonal ($A = 1/\sqrt{2}(H - V)$) ones. From the spectrum of Figure 1 c), we can estimate to couple light into the state $S \approx \sqrt{0.78}H + \sqrt{0.22}V$. Therefore, the coupling into the D state is larger than the coupling into the H state, in fact $|\langle H|S\rangle|^2 \approx 0.8$ while $|\langle D|S\rangle|^2 \approx 0.88$. Conversely, the coupling into the new auxiliary mode (A polarized) is $|\langle A|S\rangle|^2 \approx 0.09$, lower than $|\langle V|S\rangle|^2 \approx 0.22$. This results in a decrease of more than a half of the power coupled into the auxiliary mode, as visually confirmed comparing Fig. 3c and e, which is not enough to thermally stabilize the system.

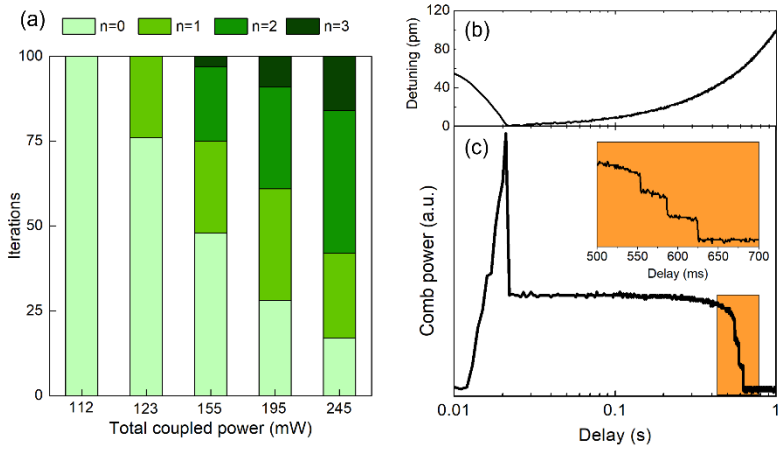

Figure 4 Panel a) shows the soliton number generation over 100 iteration for different values of total coupled power. Panel b) represents the wavelength detuning as a function of time during backward scan. Panel c) shows the corresponding power at the output of the FBG. The inset better shows the time duration of the solution steps. To increase readability, we arbitrarily set detuning = 0 at the point where the system enters the red-detuned regime.

Considering that a high soliton number can be sustained if enough power circulates in the resonator, we investigated how the soliton number statistics is modified by simply changing the total coupled power at a fixed resonance splitting of 10 pm. The results are reported in Figure 4a and show that soliton formation happens above a certain power threshold, between 112 and 123 mW in our system and, as expected, the likelihood of higher soliton number increases by increasing the coupled power. Often, the single soliton regime is the preferred state for certain applications, thanks to its smooth spectrum and well-defined repetition rate, which is very close to the cavity FSR of the resonator. Although from Fig. 3b and Fig. 4a it is possible to avoid high-order soliton states by decreasing the coupled power or increasing the splitting between the resonances, this also happens at the expenses of a low successful rate (about 25 %) of DKS formation. It has been shown [20] that a slow backward tuning of the pump from a high soliton number state can give access in sequence to all the other lower soliton states, including the n = 1. However, this has been shown in systems with longer soliton lifetime, which could be accessed with no need of any auxiliary resonance. In the present system such mechanism cannot be taken for granted, as a backward tuning of tens of picometers might cause the loss of the auxiliary resonance. We then verify that this applies to this system too, and in Fig. 4b we show that we can switch from a n = 3 state to a n = 2 and n = 1. All these states have a lifetime of tens of milliseconds, long enough to be accessed by simple laser tuning.

We then access DKS state with the highest power level over 200 iterations and we check how backward tuning modifies the soliton number statistics. Considering an initial pool consisting of 6.5% of n = 0 cases, 24% of n = 1 cases, 46% of n = 2 cases and 23.5% of n = 3 cases, the final statistics leads to 44.5% of n = 0 cases and 55.5% of n = 1 cases with no higher soliton left. As detailed in Table 1, the increased number of n = 0 cases is almost entirely given by the process n = 2 → n = 0.

Initial DKS formation	**Backward tuning from n = 2**	**Backward tuning from n = 3**	
n=3 (23.5%)			
n=2 (46%)		n=3 → n=2 (22.5%)	
n=1 (24%)	n=2 → n=1 (19.5%)	n=3 → n=1 (1%)	n=3 → n=2→ n=1 (11%)
n=0 (6.5%)	n=2 → n=0 (26.5%)		n=3 → n=2→ n=0 (11.5%)

Table 1 Soliton number generation after backward tuning from DKS formation.

3.3 Thermal tuning

Finally, we show that with this method, DKS in the microring can be accessed by keeping the wavelength of the laser fixed while tuning the cavity resonance by changing the temperature of the whole chip. Conceptually, such scheme is similar to laser tuning, however, from a technological point of view, it allows one to use fixed frequency lasers, which have a simpler monolithic design with no moving parts and can feature lower phase noise than tunable ECDL. Usually, fast and precise temperature setting is achieved by microheaters placed close to the ring [26]. However, analogously to wavelength tuning, accessing the soliton regime by thermal tuning requires that thermal scanning speed must be close to the thermal constant of the sample. This can pose a challenge for resistive heating methods, like the one used in SiN, when soliton states are very short living, such as in our sample. Instead, here we exploit the enhanced thermal stability provided by the auxiliary resonance to turn the OFC into a DKS by simply acting on the TEC placed under the chip. We placed the laser wavelength about 16.8 pm on the blue-side of the TE *C*-resonance, while the chip is stabilized at 28.5°C. Once we set the new TEC temperature to 28°C, the chip's temperature starts to decrease (Figure 5a), and the laser line progressively enters the resonance (Figure 5b). The TEC response time is several seconds, much slower than the microing's one. Once the temperature reaches 27.76 °C, the system switch to the red-detuned regime and a clear soliton step is present in the comb power time trace. The height of the soliton step and its optical spectrum indicates the formation of a DKS with n = 2. Importantly, after soliton formation, the resonance wavelength undergoes large temperature fluctuations, corresponding to about 12 pm of resonance shift, further in the red-detuned regime and back to longer wavelengths. Nevertheless, the soliton state remains stable over minutes of operation.

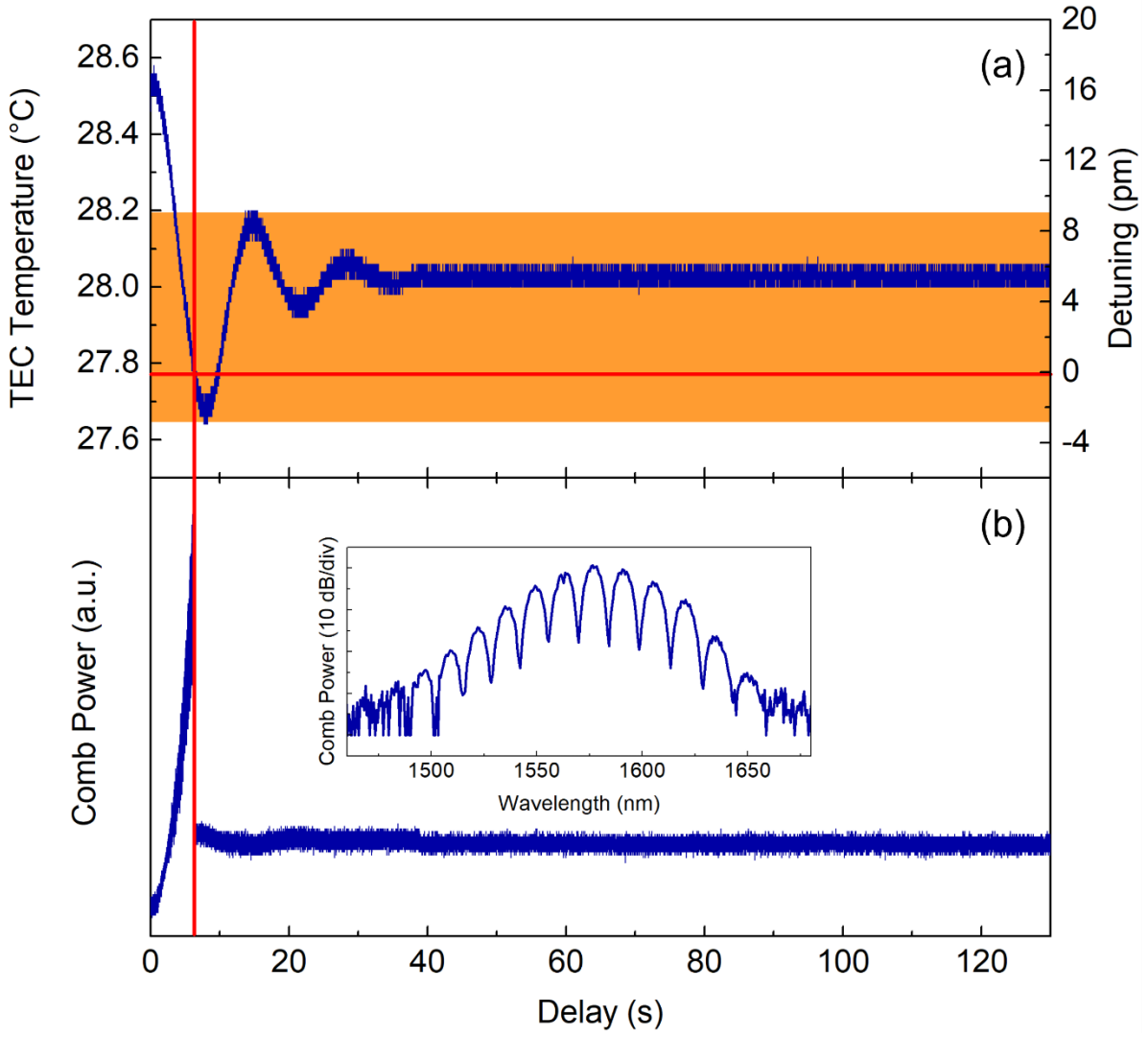

Figure 5 In a) we report the temperature red by the thermistor as a function of time. The right scale shows the corresponding detuning of the pump wavelength with respect to the point where the system enters the red-detuned regime, which is indicated by the crossing of the red lines. Panel b) reports the corresponding comb power detected at the output of the FBG, while the inset shows the envelop of the optical spectrum taken with a low-resolution grating of the OSA.

4. Conclusions

We reported an experimental method to access stable DKS states in SiN microresonators with short living soliton lifetime. Contrary to common approaches that require additional off-chip resources, such as auxiliary lasers or fast modulators and feedbacks, this scheme exploits an inherent characteristic of the resonator: its orthogonally polarized resonances. In this way, we could increase the time duration of the soliton step by four orders of magnitude, allowing easy access to the solitonic regime by simple manual laser wavelength tuning. Indeed, the presented method allows one to make the soliton lifetime independent from the time constant of the sample. We successfully achieved soliton generation by keeping the laser frequency fixed, and simply acting on the thermo-electric cooler placed beneath the sample, which has several seconds of response time, while the intrinsic soliton lifetime of the sample is less than 500 ns.

Moreover, we systematically investigated the likelihood of soliton number generation by varying the splitting between the pump and the auxiliary resonance, and the total power coupled into the chip. We could achieve soliton formation over about 95% of the iterations at best, with single soliton formation in about 19% of the cases. Then, we have shown that we can increase the percentage of single soliton formation to more than 50% by backward tuning of the pump laser.

Beside robust and straightforward soliton generation, the proposed method can lead to several important progresses in microcomb technology. In fact, the simplified pumping scheme facilitates the integration of pump laser systems on a chip [36,37], especially when fixed frequency lasers are employed, which can contribute to the realization of OFC with very low-phase noise [26]. Finally, the ability to simultaneously pump two sets of resonances with different FSR within the same resonator and using a single pump laser, opens new possibilities for exploiting this scheme for on-chip dual-comb spectroscopy [10].

5. Acknowledgment

Ministero dell'Istruzione, dell'Università e della Ricerca (Dipartimenti di Eccellenza Program (2018–2022)).
the French RENATECH network.

6. References

1. P. Del'Haye, A. Schliesser, O. Arcizet, T. Wilken, R. Holzwarth, and T. J. Kippenberg, "Optical frequency comb generation from a monolithic microresonator," Nature **450**, 1214–1217 (2007).
2. P. Del'Haye, O. Arcizet, A. Schliesser, R. Holzwarth, and T. J. Kippenberg, "Full stabilization of a microresonator-based optical frequency comb," Phys. Rev. Lett. **101**, 053903 (2008).
3. T. J. Kippenberg, S. M. Spillane, and K. J. Vahala, "Kerr-nonlinearity optical parametric oscillation in an ultrahigh-Q toroid microcavity," Phys. Rev. Lett. **93**, 18–21 (2004).
4. T. J. Kippenberg, A. L. Gaeta, M. Lipson, and M. L. Gorodetsky, "Dissipative Kerr solitons in optical microresonators," Science (80-.). **361**, (2018).
5. F. Leo, S. Coen, P. Kockaert, S. P. Gorza, P. Emplit, and M. Haelterman, "Temporal cavity solitons in one-dimensional Kerr media as bits in an all-optical buffer," Nat. Photonics **4**, 471–476 (2010).
6. T. Herr, V. Brasch, J. D. Jost, C. Y. Wang, N. M. Kondratiev, M. L. Gorodetsky, and T. J. Kippenberg, "Temporal solitons in optical microresonators," Nat. Photonics **8**, 145–152 (2014).
7. K. Saha, Y. Okawachi, B. Shim, J. S. Levy, R. Salem, A. R. Johnson, M. A. Foster, M. R. E. Lamont, M. Lipson, and A. L. Gaeta, "Modelocking and femtosecond pulse generation in chip-based frequency combs," Opt. Express **21**, 1335–1343 (2013).
8. M. G. Suh, Q. F. Yang, K. Y. Yang, X. Yi, and K. J. Vahala, "Microresonator soliton dual-comb spectroscopy," Science (80-.). **354**, 600–603 (2016).
9. M. Yu, Y. Okawachi, A. G. Griffith, N. Picqué, M. Lipson, and A. L. Gaeta, "Silicon-chip-based mid-infrared dual-comb spectroscopy," Nat. Commun. **9**, 1869 (2018).
10. A. Dutt, C. Joshi, X. Ji, J. Cardenas, Y. Okawachi, K. Luke, A. L. Gaeta, and M. Lipson, "On-chip dual-comb source for spectroscopy," Sci. Adv. **4**, 1–10 (2018).
11. E. Obrzud, M. Rainer, A. Harutyunyan, M. H. Anderson, J. Liu, M. Geiselmann, B. Chazelas, S. Kundermann, S. Lecomte, M. Cecconi, A. Ghedina, E. Molinari, F. Pepe, F. Wildi, F. Bouchy, T. J. Kippenberg, and T. Herr, "A microphotonic astrocomb," Nat. Photonics **13**, 31–35 (2019).
12. M. H. P. Pfeiffer, C. Herkommer, J. Liu, H. Guo, M. Karpov, E. Lucas, M. Zervas, and T. J. Kippenberg, "Octave-spanning dissipative Kerr soliton frequency combs in Si3N4 microresonators," Optica **4**, 684 (2017).
13. V. Brasch, E. Lucas, J. D. Jost, M. Geiselmann, and T. J. Kippenberg, "Self-referenced photonic chip soliton Kerr frequency comb," Light Sci. Appl. **6**, e16202-6 (2017).

14. P. Del'Haye, A. Coillet, T. Fortier, K. Beha, D. C. Cole, K. Y. Yang, H. Lee, K. J. Vahala, S. B. Papp, and S. A. Diddams, "Phase-coherent microwave-to-optical link with a self-referenced microcomb," Nat. Photonics **10**, 516–520 (2016).
15. Z. L. Newman, V. Maurice, T. Drake, J. R. Stone, T. C. Briles, D. T. Spencer, C. Fredrick, Q. Li, D. Westly, B. R. Ilic, B. Shen, M.-G. Suh, K. Y. Yang, C. Johnson, D. M. S. Johnson, L. Hollberg, K. J. Vahala, K. Srinivasan, S. A. Diddams, J. Kitching, S. B. Papp, and M. T. Hummon, "Architecture for the photonic integration of an optical atomic clock," Optica **6**, 680 (2019).
16. J. Pfeifle, V. Brasch, M. Lauermann, Y. Yu, D. Wegner, T. Herr, K. Hartinger, P. Schindler, J. Li, D. Hillerkuss, R. Schmogrow, C. Weimann, R. Holzwarth, W. Freude, J. Leuthold, T. J. Kippenberg, and C. Koos, "Coherent terabit communications with microresonator Kerr frequency combs," Nat. Photonics **8**, 375–380 (2014).
17. P. Marin-Palomo, J. N. Kemal, M. Karpov, A. Kordts, J. Pfeifle, M. H. P. Pfeiffer, P. Trocha, S. Wolf, V. Brasch, M. H. Anderson, R. Rosenberger, K. Vijayan, W. Freude, T. J. Kippenberg, and C. Koos, "Microresonator-based solitons for massively parallel coherent optical communications," Nature **546**, 274–279 (2017).
18. P. Trocha, D. Ganin, M. Karpov, M. H. P. Pfeiffer, A. Kordts, J. Krockenberger, S. Wolf, P. Marin-Palomo, C. Weimann, S. Randel, W. Freude, T. J. Kippenberg, and C. Koos, "Ultrafast optical ranging using microresonator soliton frequency combs," Science (80-.). **359**, 887–891 (2018).
19. J. Liu, E. Lucas, A. S. Raja, J. He, J. Riemensberger, R. N. Wang, M. Karpov, H. Guo, R. Bouchand, and T. J. Kippenberg, "Photonic microwave generation in the X- and K-band using integrated soliton microcombs," Nat. Photonics **14**, (2020).
20. H. Guo, M. Karpov, E. Lucas, A. Kordts, M. H. P. Pfeiffer, V. Brasch, G. Lihachev, V. E. Lobanov, M. L. Gorodetsky, and T. J. Kippenberg, "Universal dynamics and deterministic switching of dissipative Kerr solitons in optical microresonators," Nat. Phys. **13**, 94–102 (2017).
21. N. G. Pavlov, S. Koptyaev, G. V. Lihachev, A. S. Voloshin, A. S. Gorodnitskiy, M. V. Ryabko, S. V. Polonsky, and M. L. Gorodetsky, "Narrow-linewidth lasing and soliton Kerr microcombs with ordinary laser diodes," Nat. Photonics **12**, 694–698 (2018).
22. S. Zhang, J. M. Silver, L. Del Bino, F. Copie, M. T. M. Woodley, G. N. Ghalanos, A. Ø. Svela, N. Moroney, and P. Del'Haye, "Sub-milliwatt-level microresonator solitons with extended access range using an auxiliary laser," Optica **6**, 206 (2019).
23. J. R. Stone, T. C. Briles, T. E. Drake, D. T. Spencer, D. R. Carlson, S. A. Diddams, and S. B. Papp, "Thermal and Nonlinear Dissipative-Soliton Dynamics in Kerr-Microresonator Frequency Combs," Phys. Rev. Lett. **121**, 63902 (2018).
24. Z. Lu, W. Wang, W. Zhang, S. T. Chu, B. E. Little, M. Liu, L. Wang, C. L. Zou, C. H. Dong, B. Zhao, and W. Zhao, "Deterministic generation and switching of dissipative Kerr soliton in a thermally controlled micro-resonator," AIP Adv. **9**, (2019).
25. L. Razzari, D. Duchesne, M. Ferrera, R. Morandotti, S. Chu, B. E. Little, and D. J. Moss, "CMOS-compatible integrated optical hyper-parametric oscillator," Nat. Photonics **4**, 41–45 (2010).
26. C. Joshi, J. K. Jang, K. Luke, J. Xingchen, S. A. Miller, A. Klenner, Y. Okawachi, M. Lipson, and A. L. Gaeta, "Thermally controlled comb generation and soliton modelocking in microresonators," Opt. Lett. **41**, 1–4 (2016).
27. H. Zhou, Y. Geng, W. Cui, S. W. Huang, Q. Zhou, K. Qiu, and C. Wei Wong, "Soliton bursts and deterministic dissipative Kerr soliton generation in auxiliary-assisted microcavities," Light Sci. Appl. **8**, (2019).
28. J. Liu, A. S. Raja, M. Karpov, B. Ghadiani, M. H. P. Pfeiffer, D. Botao, N. J. Engelsen, H. Guo, M. Zervas, and T. J. Kippenberg, "Ultralow-power chip-based soliton microcombs for photonic integration," Optica **5**, 1347–1353 (2019).
29. J. S. Levy, A. Gondarenko, M. A. Foster, A. C. Turner-foster, A. L. Gaeta, and M. Lipson, "CMOS-compatible multiple-wavelength oscillator for on-chip optical interconnects," Nat. Photon. **4**, 2–5 (2010).
30. T. Carmon, L. Yang, and K. J. Vahala., "Dynamical thermal behavior and thermal self-stability of microcavities," Opt. Express **12**, 4742–4750 (2004).
31. A. Billat, D. Grassani, M. H. P. Pfeiffer, S. Kharitonov, T. J. Kippenberg, and C.-S. Brès, "Large second harmonic generation enhancement in Si3N4 waveguides by all-optically induced quasi-phase-matching," Nat. Commun. **8**, 1016 (2017).
32. V. A. Gritsenko, S. S. Nekrashevich, V. V. Vasilev, and A. V. Shaposhnikov, "Electronic structure of memory traps in silicon nitride," Microelectron. Eng. **86**, 1866–1869 (2009).
33. V. Brasch, M. Geiselmann, M. H. P. Pfeiffer, and T. J. Kippenberg, "Bringing short-lived dissipative Kerr soliton states in microresonators into a steady state," Opt. Express **24**, 29312 (2016).
34. T. Wildi, V. Brasch, J. Liu, T. J. Kippenberg, and T. Herr, "Thermally stable access to microresonator

solitons via slow pump modulation," Opt. Lett. **44**, 4447 (2019).
35. Q. Li, T. C. Briles, D. A. Westly, T. E. Drake, J. R. Stone, B. R. Ilic, S. A. Diddams, S. B. Papp, and K. Srinivasan, "Stably accessing octave-spanning microresonator frequency combs in the soliton regime," Optica **4**, 193 (2017).
36. B. Stern, X. Ji, Y. Okawachi, A. L. Gaeta, and M. Lipson, "Battery-operated integrated frequency comb generator," Nature **562**, 401–405 (2018).
37. A. S. Raja, A. S. Voloshin, H. Guo, S. E. Agafonova, J. Liu, A. S. Gorodnitskiy, M. Karpov, N. G. Pavlov, E. Lucas, R. R. Galiev, A. E. Shitikov, J. D. Jost, M. L. Gorodetsky, and T. J. Kippenberg, "Electrically pumped photonic integrated soliton microcomb," Nat. Commun. **10**, 1–10 (2019).